IEEE Access
Multidisciplinary | Rapid Review | Open Access Journal

Received May 20, 2021, accepted May 31, 2021, date of publication June 11, 2021, date of current version June 21, 2021.

Digital Object Identifier 10.1109/ACCESS.2021.3088431

Highly Sensitive Nondestructive Tunneling Magneto Resistive Imaging: Simulation and Experimental Validation

JOONGHO AHN, (Graduate Student Member, IEEE), JINHWAN BAIK, CHULHONG KIM, (Senior Member, IEEE), AND SUNG-MIN PARK, (Member, IEEE)

Department of Convergence IT Engineering, Electrical Engineering, and Mechanical Engineering, Pohang University of Science and Technology, Pohang 37673, South Korea
Medical Device Innovation Center, Pohang University of Science and Technology, Pohang 37673, South Korea

Corresponding authors: Chulhong Kim (chulhong@postech.edu) and Sung-Min Park (sungminpark@postech.ac.kr)

This work was supported in part by the Ministry of Science and ICT (MSIT), South Korea, under the ICT Creative Consilience Program supervised by the Institute for Information and communications Technology Planning and Evaluation (IITP) under Grant IITP-2020-2011-1-00783, in part by the Basic Science Research Program through the National Research Foundation of Korea (NRF) by the Ministry of Education under Grant 2020R1A6A1A03047902, and in part by the National Research and Development Program through the National Research Foundation of Korea (NRF) funded by the Ministry of Science and ICT under Grant 2020M3H2A1078045.

ABSTRACT With the increased use of high-performance thin steels, detecting internal or external micro defects in a manufacturing process has become critical for the steel manufacturing process's cost and quality management. For detecting defects, magnetic-based nondestructive testing (NDT) methods have been researched widely due to their simplicity, ease of use, and contactless nature. However, magnetic-based approaches suffer from low sensitivity, thus limiting their use. Here, we present a highly sensitive tunneling magnetoresistive (TMR) imaging system to detect sub-surface defects in thin steel samples. Artificially created holes in the steel plates were magnetically imaged by measuring magnetic flux leakage (MFL). The experimental results were compared against the simulated results to confirm the visibility of the holes. We also confirmed the successful visualization of the sub-surface defects in the steel plates formed during the real manufacturing processes. Thus, based on these results, we believe the TMR method holds great potential as an NDT technique for steel manufacture management.

INDEX TERMS Magnetic flux leakage, magnetic sensor, nondestructive testing, steel, tunneling magnetoresistance.

I. INTRODUCTION

The demands for thin but durable steel has been rapidly increasing due to the recent trend of lightweight industrial products such as automobile [1]. While this trend is sound for green and economical solutions, the quality controls in steel manufacturing processes, however, it becomes more challenging. While manufacturing thin steels, unintended inclusions of impurities such as air, oxide, and sulfides would result in defects during rolling processes [2]. Thus, the fabricated steels with the defects have the potential risks of getting broken or degraded. The nondestructive detection of such a small defect in real-time, i.e., online, has been identified as a key quality management solution.

Various nondestructive testing (NDT) techniques have been researched and utilized to identify defects without destructing steel samples. Each method has different pros and cons, depending upon the principles of operation [3]. A liquid penetrant inspection is a low-cost and straightforward approach. However, it is only limited to detecting defects on the clean surface since liquid penetrant may not be able to wipe clean on a rough surface [4]. A magnetic particle inspection is simple and low cost and can detect surface and sub-surface defects [5]. However, this technique is useful for only ferromagnetic materials such as steel. Radiographic testing helps detect both surface and shallow internal defects [6] but cannot detect flaws that are not along the radiation

The associate editor coordinating the review of this manuscript and approving it for publication was Ravibabu Mulaveesala.

directions [7]. In addition to technical limitations, the above methods have potential safety issues on the system operator due to the usage of chemicals, magnetic powders, or ionizing radiation [7], [8].

As an alternative, an eddy current testing has been applied to detect defects in various types of steel, including tubes and rods [9]. However, it is only applicable to sensitive electric conductors, and skin effect limits its use to detect internal defects [10]. The 3D high-resolution sonographic methods have also been investigated as safe, easy, and simple techniques for detecting relatively deep internal defects [11]. However, the nature of ultrasound requires an acoustic coupling medium (e.g., water) to propagate, which is a big hurdle for online screening [12].

A magnetic flux leakage (MFL) method is similar to magnetic particle inspection [13] but uses magnetic sensors instead of the magnetic powders. The principles of the MFL is as follows: magnetic fields are applied continuously to the steel using electromagnets, and the defects distort the magnetic fields locally, causing the leakage of magnetic fields, which are subsequently detected by the magnetic sensors to localize the defects. Typically, Hall effect, anisotropic magnetoresistance (AMR) or giant magnetoresistance (GMR) sensors have been used for the MFL approach [13]. Thanks to the non-contact configuration, the adaptation of MFL is steadily increasing to inspect samples in real industrial sites or in objects under motion [14]–[19]. However, MFL still cannot detect micro defects reliably due to the low sensitivity of the magnetic sensors limiting their wide-spread use in real manufacturing procedures.

Recently, highly sensitive tunneling magneto resistive (TMR) sensors have been developed. The TMR sensors have magnetic tunnel junction (MTJ), called a TMR element, which consists of free ferromagnetic and stationary ferromagnetic layers separated by a thin insulating barrier [20], [21]. The free layer reacts readily to the external magnetic fields, while the fixed layer does not. Since two layers respond differently to the external magnetic field, a relative orientation of the magnetic moments in the two layers gets created, causing the tunneling effect for electrons passing through the barrier. The change in the current generated by the external magnetic field is called tunneling magnetoresistance, and is linear with the change in the external magnetic field. The TMR sensors have better sensitivity, better thermal stability, consumes low power compared to the previously mentioned magnetic sensors [21], [22]. With these advantages of the TMR sensors, TMR-based NDT methods have been studied to detect small defects (Table 1) [23]–[26]. These studies targeted samples with various types but only surface defects. However, in the process of manufacturing steels, detecting internal defects are also important because they would affect the quality of steels in subsequent stages [27]. Nevertheless, due to the difficulty to procure steel samples containing sub-surface defects by inclusions, limited research has been conducted with steel samples with artificially-created defects [28].

The primary objective of this study was to propose a sensitive steel defect detecting system that can identify both surface and sub-surface defects created by impurities during the general manufacturing process. We developed a magnetic flux imaging system that employs a high-sensitive TMR sensor to detect defects. Using this system, we magnetically detected artificial holes and compared the experimental results with the simulated results under similar conditions. In addition, we successfully imaged the sub-surface defects formed in the real-world steel sample using this system. Our findings suggest that the highly sensitive TMR imaging with data analysis equipment could be considered as a future NDT technique for the steel manufacturing processes.

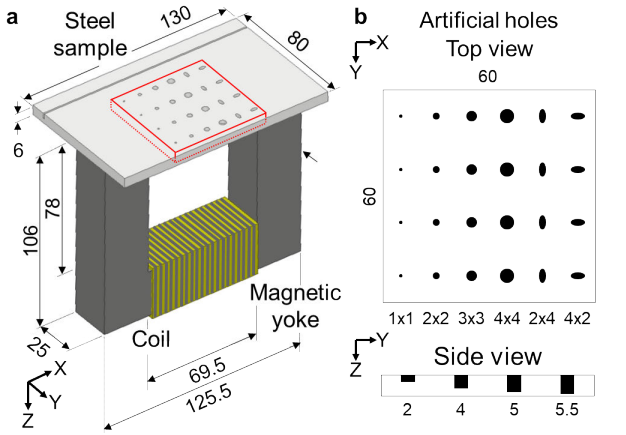

FIGURE 1. Finite element method simulation. (a) Simulation configuration including a magnetic coil, a magnetic yoke, and a steel sample. Region of imaging (ROI) is marked with red-lined cubic box. (b) Top and side views of the steel sample with various artificial holes. Unit, mm.

II. MATERIALS AND METHODS

A. FINITE ELEMENT METHOD SIMULATION

A magnetic field simulation was performed using electromagnetic field simulation software (ANSYS Maxwell, ANSYS Inc., PA, USA). Figure 1a shows a 3D simulation model comprising of an excitation coil, a magnetic yoke, and a steel sample with several holes. The magnetic yoke was designed with the dimensions of 25 mm wide, 106 mm high, and 125.5 mm long. The simulator parameters are summarized in Table 1. A direct current of 15 A was applied to the coil, which generates a magnetic field of about 18 G between the two pillars of the magnetic yoke. The magnetic yoke's relative permeability and the steel sample were set to 5,000 and 40, respectively [18], [29]. Figure 1b shows the steel sample's top and side views with the 24 cylindrical or elliptical shaped surface holes. The sizes of the holes are also detailed in Fig. 1b. The magnetic field profiles along the X-axis were extracted at 1 mm above the sample's surface to analyze the magnetic flux leakage.

B. MAGNETIC FLUX IMAGING (MFI) SYSTEM USING A TMR SENSOR

We developed a magnetic flux imaging (MFI) system using the TMR sensor. The schematic of the MFI system is shown

TABLE 1. Summary of targeted defects on the state-of-the-art studies using tmr sensors.

	B. Wu, et al. [23] (2015)	K. Tsukada, et al. [24] (2018)	B. Wang, et al. [25] (2018)	J. Zhang, et al., [26] (2020)	This study
Position of defects	Surface	Surface	Surface	Surface	Surface and subsurface
Cause of defects	Artificial	Artificial	Inclusion	Broken	Inclusion
Sample	Wire rope	Steel plate	Steel sheet	Wire rope	Steel sheet
Method	Magnetic flux leakage	Eddy current	Magnetic flux leakage	Magnetic flux leakage	Magnetic flux leakage

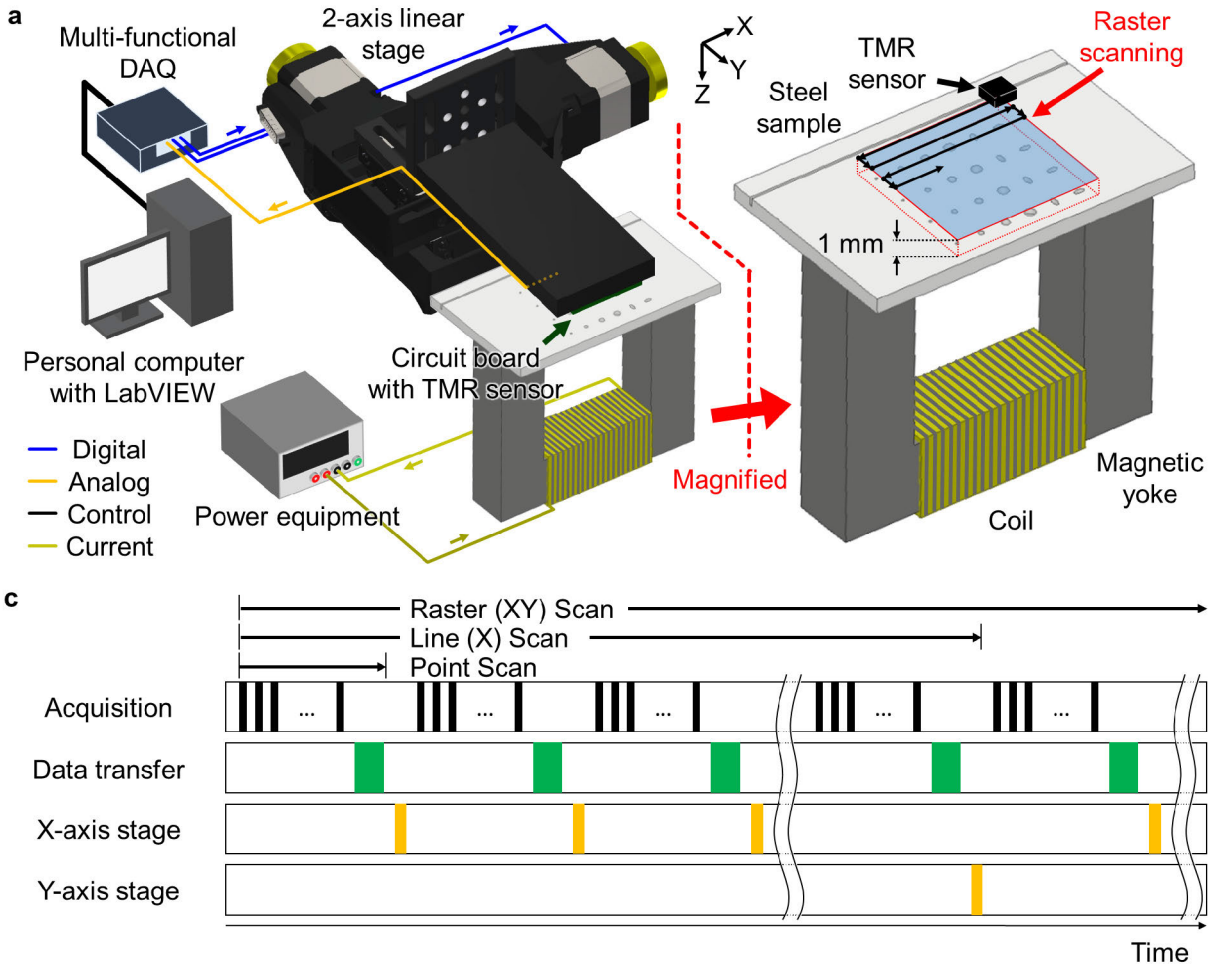

FIGURE 2. (a) Schematic of a magnetic flux imaging (MFI) system using a TMR sensor. (b) Experimental flow. (c) Timing diagram for imaging sequences. TMR, tunneling electro-resistance; DAQ, data acquisition; AI, analog input; and DO, digital output.

TABLE 2. Summary of the simulation parameters.

	Coil (perfect conductor)	Magnetic yoke (ferrite)	Steel Sample (S45C)	Hole (air)
Relative Permeability	1	5,000	40	1
Conductivity [S/m]	1×10^{30}	0.01	1.1×10^{5}	0

in Fig. 2a. The system's core functionality includes the continuous magnetizing of a sample, the motorized raster scanning, and the magnetic sensing. The key improvements of this system over conventional MFI systems [28] is the use of a highly sensitive TMR sensor, automated scanning, and an algorithm for visualizing defects. The experimental flow is shown in Figure 2b.

First, a magnetic source was fabricated by wrapping a coil on a U-shaped magnetic yoke (UU126, Tangda Technology CO., Ltd., China) with 200 turns. A power equipment (E3632A, Agilent Technologies Inc., CA, USA) was used to supply a direct current to the coil to induce magnetic fields. The induced magnetic field is transmitted to a steel sample with relatively high permeability compared to air, magnetizing the sample. The sample was kept magnetized throughout the experiment by continuously supplying the

current to the coil. TMR linear sensor (TMR2901, MultiDimension Technology CO., Ltd., China) was placed to measure the magnitude of the magnetic fields in the X direction, which is the same as the direction of the induced magnetic field. The magnetic fields leaked out of the sample at the site of defects were detected by the TMR sensor. The differential output of the TMR sensor was acquired by the analog input channel of a multi-functional data acquisition (DAQ) board (PCIe-6321, National Instruments Corp., TX, USA). The TMR sensor was fixed on two motorized linear stages (L-509, Physik Instrumente GmbH & Co. KG, Germany), which uses a stepper motor to move the stage. The data acquisition was performed using the DAQ board. The TMR sensor's scanning sequence and the movement for the motorized stages were implemented using LabVIEW (National Instruments Corp., TX, USA). The timing diagram for the DAQ and raster scanning sequences is presented in Fig. 2c. At each location, 100 magnetic signals were acquired from the TMR sensor. The acquired data were transferred to the LabVIEW, where they get averaged and accumulated in data storage. After completing signal acquisition at one position, the stage was moved to the next position to acquire the next set of data. This point scan sequence is repeated in the raster scan to create a 2D image. The postprocessing was performed in MATLAB (MathWorks Inc., MA, USA).

C. MFI OF ARTIFICIAL SAMPLES

To validate the MFI system, two steel sample were prepared. One is a 150 μm-wide slit that was created using a laser. The other is the 24 artificial holes that were made using precise machining on an S45C steel plate (steel with 0.45% carbon), of which dimensions are the same as those in Fig. 1b. The region of interest (ROI) was aligned on the center of the magnetic source. After aligning, the steel sample was magnetized by supplying direct current to the coil. After the steel sample was magnetized sufficiently and is attached firmly to the magnetic yoke, the TMR sensor was positioned 1 mm above the steel sample's surface. Then magnetic flux imaging was performed by scanning the sample with a step size of 500 μm.

D. MFI OF A REAL SAMPLE

An industrial sample that is a 1.7 mm-thick half-finished cold-rolled steel sheet manufactured by POSCO (Pohang Iron & Steel Company CO., Ltd., Republic of Korea) was prepared. The defects were formed during a rolling process, which is a part of the steel thinning process. Then magnetic imaging of the sample was performed with a step size of 200 μm. Additionally, a repeated imaging experiment was conducted with a Hall sensor (WSH202, Winson semiconductor Corp., Taiwan) instead of the TMR sensor to directly compare the performance between the TMR and Hall sensors.

III. RESULTS

A. SYSTEM VALIDATION AND CHARACTERIZATION

To validate and characterize the MFI system, the steel sample with the 150 μm-wide slit was imaged (Fig. 3).

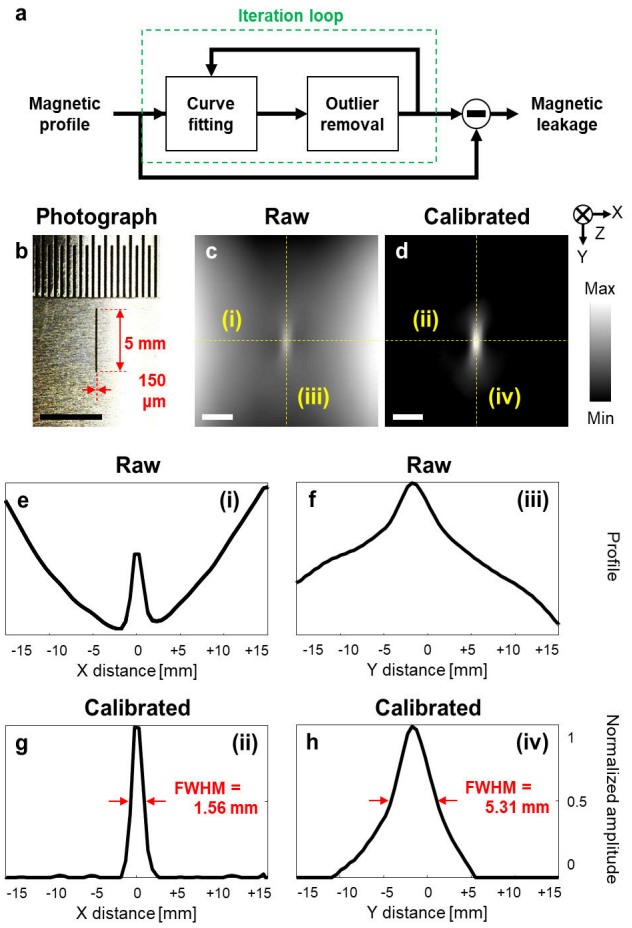

FIGURE 3. Magnetic flux imaging (MFI) of a 150-μm slit. (a) Curve-fitting and outlier removal algorithm. (b) Photograph, (c) raw, and (d) corrected magnetic flux images of the slit. (e-f) Raw profiles acquired along the lines "i" and "iii" in (c), respectively. (g-h) Corrected profiles acquired along the lines "ii" and "iv" in (d), respectively. FWHM, full width at half maximum. All scale bars are 5 mm.

For visualizing the slit, it is necessary to extract only the change in the defect's magnetic field. Stronger magnetic fields are measured within the slit than the surroundings due to local distortion. However, the background magnetic field is not homogeneous within the ROI. Thus, an iterative curve-fitting and outlier removal algorithm was applied along the X-axis to extract the magnetic field (Fig. 3a). In the curve-fitting step, the magnetic profile is fitted to a polynomial, based on the linear absolute deviation (LAD) method, as follows [30]:

$$\frac{1}{n}\sum_{i=0}^{n-1} w_i |f(x_i) - y_i| \tag{1}$$

where n is the number of measured samples, w_i is the i^{th} weight for the sample, $f\ (x_i)$ is the i^{th} value of the fitted curve, and y_i is the i^{th} value of measured signals. The LAD method finds $f\ (x)$ by minimizing the deviation. In the subsequent step, the values forming the unusual patterns, i.e., outliers, are removed. The magnetic leakage is then extracted

by calculating the difference between the original profiles and outlier-removed profiles. The successfully imaged slit is shown in Figs. 3b–d. The MFL by the slit is clearly visualized in the raw and corrected data (Fig. 3c-d) and matches well with the original photograph (Fig. 3b). The 1D profiles acquired along the lines "i" and "iii" in Fig. 3c (i.e., raw image) are shown in Figs. 3e–f, respectively. The corrected 1D profiles obtained along the lines "ii" and "iv" in Fig. 3d are shown in Figs. 3g–h, respectively. The full widths at half maxima (FWHMs) are estimated to be 1.56 and 5.31 mm along the X and Y axes, respectively. Thus, the lateral resolution is approximately 1.5 mm at 1 mm above the sample surface. The imaging speed for the imaging area of 30×30 mm^2 with a 500 μm interval was about 12 minutes. This speed depends on the imaging area, the step size, and the number of averaging employed. The signal-to-noise ratio (SNR), defined as the ratio between the maximum value on the slit position over the standard deviation of the background noise, is calculated to be 39.3 dB.

B. MFI OF ARTIFICIAL HOLES: SIMULATION VS. EXPERIMENTAL RESULTS

The comparison images of simulated and experimental magnetic flux (MF) of the steel plate with artificial holes are shown in Fig. 4. In both simulated and experimentally acquired images, the holes (Fig. 1b) are clearly identified, and the simulation results agree well with the experimental ones (Figs. 4a-b). The simulated 1D profiles acquired along the lines "i" and "ii" in Fig. 4a are shown in Figures 4c–d, respectively. The experimentally obtained 1D profiles obtained along the lines "iii" and "iv" in Fig. 4b are shown in Figures 4e–f, respectively. The 1D profiles along X and Y axes in the simulation and experimental results show similar patterns as well. To evaluate the similarity, we represented the corresponding pair of pixel values on a scatter diagram, as shown in Fig. 4g, and calculated the correlation coefficient. The correlation coefficient was 0.93 (Fig. 4g), which is very high, thus indicating that the magnetic flux on simulated and experimental results are similarly distributed [31]. Further, the FWHMs (Fig. 4h) and normalized MF signal amplitudes (Fig. 4i) were quantitatively compared between the simulated and experimental results. The two quantified parameters have a similar tendency, with the simulated results being ideal than the experimental ones. In Figure 4h, the FWHMs are linear along the X-axis, i.e., along the lengths of the holes, since the steel plate was magnetized along the X-axis by the magnetic generator. Interestingly, the FWHM of the ⑥ hole (i.e., 4×2 ellipse) is estimated to be less than 4 mm. This underestimation is mainly related to the magnetic poles that are formed locally around the hole. The ⑥ hole is on the pillar side of the magnetic generator, where the magnetic field radiates spatially, and the magnetic field obliquely affects the hole.

Unlike the FWHMs, the MF signal amplitude is more affected by the Y-axis length of a hole when the source magnetic field is applied along the X-axis. In this study, the amount of magnetic flux per unit surface is constant, and thus the MF signal amplitude is the product of the constant magnetic flux and the surface size of a hole along the Y-axis. Therefore, the largest hole ⑤ (2×4 ellipse) with a Y-axis area size of 4 mm showed the largest MF signal amplitude. In addition, the effects of the hole sizes on the magnetic poles along the X, Y and Z axes were also confirmed through simulations with all other variables controlled (Supplementary Figs. S1a-b). As the height of the hole increases (Supplementary Fig. S6c), the MF signals of the four ② holes become saturated. However, the MF signal of the ②^4 hole was smaller than the ②^2 and ②^3 holes due to the boundary effects of the magnetic field near the edges of the steel plate. The boundary effect was observed in both simulated and experimental profiles, as shown in Figs. 4d and f. The simulated and experimental results also showed good agreement when the amplitudes of FWHMs and MF signals were compared. Thus, both experimental and simulation results validate our proposed MFI system using the TMR sensor. Next, the system and algorithm were evaluated on industrial steel plates with multiple defects.

C. MFI OF REAL DEFECTS GENERATED DURING STEEL MANUFACTURING PROCESSES

The real defects in an industrial sample were evaluated using the MFI system. The defective plates were primarily sorted out by a field engineer, and the sample expected to have subsurface defects was picked out by the quality management department for evaluation. Shown in Figure 5a is the picture of the real-world sample that contains two line-shaped defects in the rolling direction. While the left defect line in the sample could be clearly identified on the bare eye, the right defect line was clear only at the top ('i' in Fig. 5) but became unclear toward the bottom ('ii' in Fig. 5). One of the defects indicated by the black arrows includes both surface and sub-surface defects. The defects identified by the MF imaging using the TMR and Hall sensors are demonstrated in Figs. 5b and c, respectively. In order to evaluate the difference between magnetic flux of surface defects vs subsurface defects, we acquired the 1D profiles along the lines "i" and "ii" as shown in Figs. 5d and e, respectively. The MF imaging taken with the TMR sensor clearly visualized both line defects due to its high sensitivity, but the image taken with the Hall sensor did not clearly show the sub-surface defect.

IV. DISCUSSION

As the demand for the high-performance steel steadily increases, the steelmakers are facing challenges related to quality control. With the increasing quality standards of steel products, finding defects non-destructively still remains a large challenge. For meeting the demanding standards, different NDT methods can be selected depending on multiple factors such as the nature of targeted samples and inspection environment. The MFL method would be more appropriate for a thin steel plate target since it can detect both

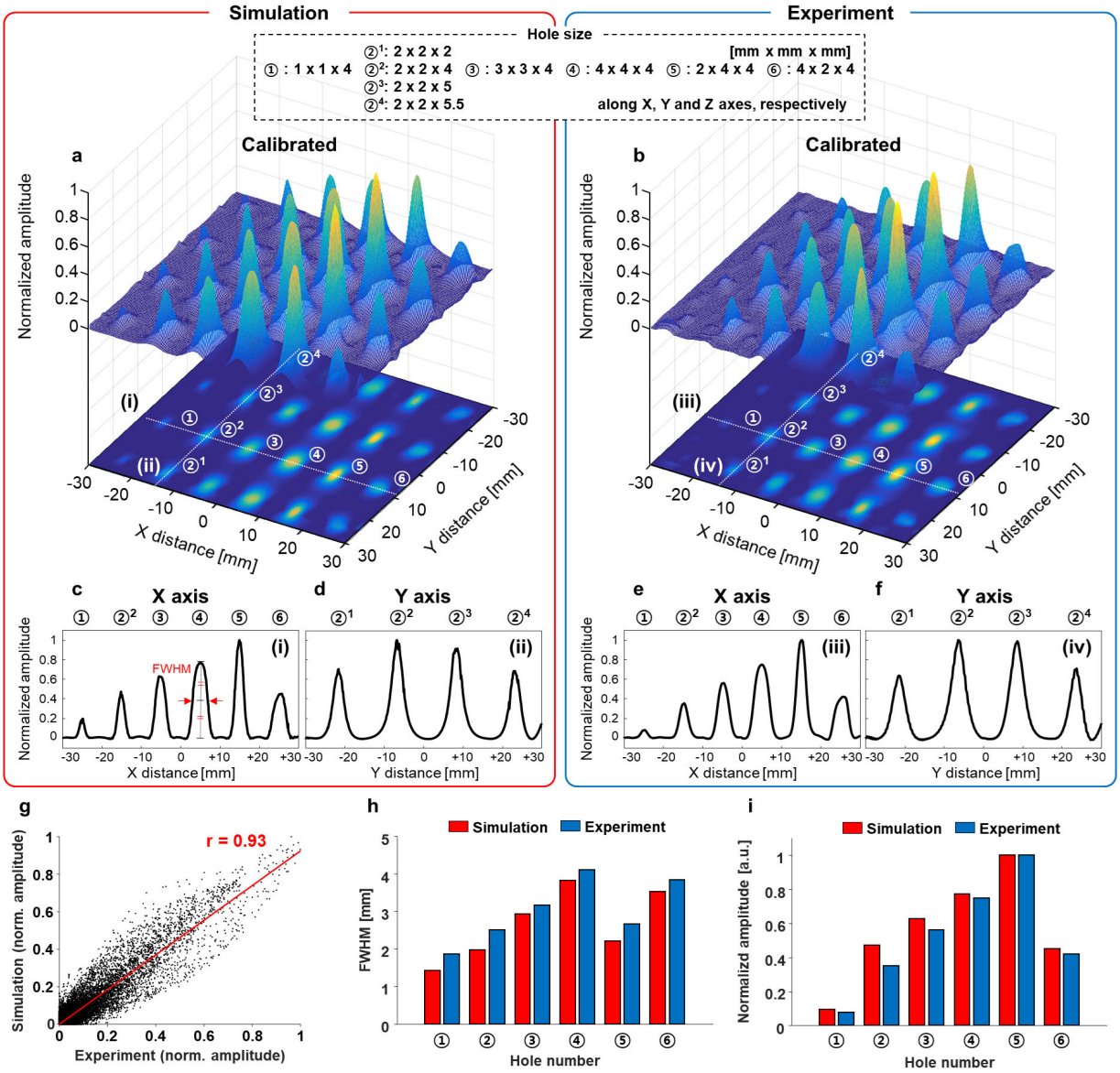

FIGURE 4. Simulation and experimental results of magnetic flux (MF) imaging of artificial holes in a steel plate. (a) Simulated and (b) experimental MF images of the artificial holes. (c-d) Corrected profiles along the lines "i" and "ii" in (a), respectively. (e-f) Corrected profiles along the lines "iii" and "iv" in (a), respectively. (g) Scatter diagram of the MF signals in (a) and (b). The correlation coefficient between the two images is 0.93 and the images are strong similarity. (h) Comparison of the FWHMs estimated from (c) and (e). (h) Comparison of the normalized amplitudes calculated from (c) and (e). FWHM, full width at half maximum.

surface and subsurface defects. As the quality of standards increases, the requirements to detect smaller defects would also increase. Here we propose the MFI system based on the commercially available TMR sensor, which enhances the magnetic field imaging sensitivity of MFI and is also optimized for NDT testing of cold-rolled sheets. In addition, compared to conventional sensors, the TMR sensors have better linearity, high thermal stability, and consume low power, thus making them more suitable for solving practical issues during NDT testing.

We validated the proposed MFI system by imaging and simulating the magnetic flux of the steel plate with the 150 μm-wide slit. To extract the change in the magnetic fields at the slit, the iterative method with a curve-fitting and outlier removal algorithm was proposed. The MFI system and method successfully visualized the slit and showed that the system could achieve a high resolution of approximately 1.5 mm lateral resolution at 1 mm above the sample surface. The finite element-based numerical simulation and imaging artificially created holes in a plate showed that the proposed MFI system and algorithm could be applied to a steel plate with multiple defects. Additional simulations were conducted to evaluate the effect of hole sizes on the MF signal in the well-controlled environments. It is confirmed that the

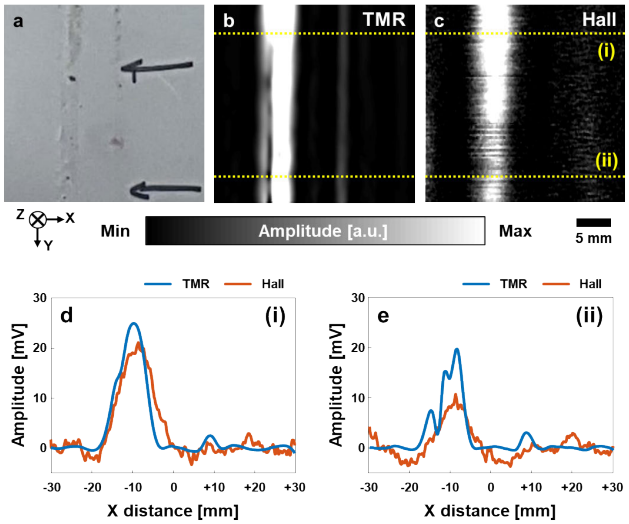

FIGURE 5. Magnetic flux imaging (MFI) of defects formed during real manufacturing processes (a) Photograph and (b-c) magnetic flux images of the defects using TMR and Hall sensor. (d-e) Profiles along the lines "i" and "ii" in (b) and (c), respectively.

simulated and experimental results are consistent, even in the phenomenon caused by the boundary effect. Then, the MFI system was applied to detect defects in the steel plate at actual manufacturing sites. Since it is difficult to find a sample with only internal defects, the sample with both surface and sub-surface defects was prepared with experts working in the steel manufacturing sites. The defect pattern shown in Fig. 5a is generally formed during the rolling process, i.e., thinning the steel, where relatively large internal defects are crushed and scattered in the rolling direction. The MF imaging taken with the TMR sensor showed that the system could detect more defects than those seen in the photograph (Fig. 5). Considering the MFI system's spatial resolutions, these results imply that our MFI system is capable of detecting both the surface and the sub-surface defects. The same imaging experiment was also performed using a Hall sensor to compare the performance. As presented in the Results, the TMR sensor with high sensitivity could detect the sub-surface defects while the Hall sensor could not perform. In addition, the Hall sensor also showed signal variation resulting from poor measurement resolution due to its low sensitivity. This signal variation using the Hall sensor also produced curve fitting errors, which made it difficult to extract the defect-induced changes. These results demonstrate that the proposed TMR system can detect the sub-surface defects that cannot be identified with the Hall system. Our findings are so far based on simulation, experiments and one real world sample testing. It is difficult to procure real world samples, but we will be coordinating with the steel companies to procure more defective real-world samples for further testing in a near future.

When conducting experiments using the proposed MFI system, it is important to consider multiple factors: (1) The TMR sensor has a trade-off relationship between the sensitivity and the saturation field, i.e., when sensitivity is high, it can sense the low magnetic field and vice versa. On the MF imaging of the industrial sample, the magnetic fields were beyond linear region of the TMR sensor and output saturated. Thus, it is necessary to select an appropriate sensor and calibrate it to ensure that the magnetic field is not saturated considering sensors' linearity and saturation field. (2) The steel samples need to be as s flat as possible: The steel sample is cut to a small piece for testing, and the sample is inevitably bent or warped during cutting. This deformation makes it difficult to maintain a specific certain distance between the sample and the sensor. Besides, improperly sized samples may cause the boundary effects of the magnetic fields within MF imaging areas. (3) The proposed algorithm was applied along X axis only because magnetic field was leaked by defects occurred along X axis. The MF image was created by accumulating the X-axis profiles only. Thus, the profiles along Y axis are incomplete. The 2-axis induction and sensing of magnetic fields are required to capture both X and Y axis. (4) The scanning speed shall be in the signal processing stage. The MFL testing can be largely affected by the velocity effect, and the induced eddy current density due to the relative velocity between the sensor and the sample under test. Therefore, the signal distortion due to this velocity effect shall be considered in further applications.

V. CONCLUSION

In this study, we developed the MFI system using the recently-commercialized TMR sensor. This system for NDT features the TMR sensor's high sensitivity, automatic scanning with fully-synchronized sequence, and the proposed signal processing algorithm that selectively extracts the MF signal leaked by defects. Our approach and methodology were validated by comparing the simulated and experimental results of the artificially created holes. Further, the defects occurred during the steel manufacturing processes were identified. This study has demonstrated that the state-of-the-art TMR sensors could be used for localizing the defects in the MFL method. From its industrial applicability, the imaging system could be extended from the sample inspection to online inspection. Array-typed TMR sensors or conveyor belts used to transport steel sheets during the steel manufacturing, can be used for a faster scan. Realizing the online imaging inspection requires more multidisciplinary accesses, engineering efforts, and verification that the proposed method is better than other NDT methods, but it would bring tremendous economic benefits to the steel industry.

ACKNOWLEDGMENT

(Joongho Ahn and Jinhwan Baik contributed equally to this work.)

REFERENCES

[1] (Mar. 2019). *Non-Destructive Testing and Inspection Market by Technique (Visual Testing, Magnetic Particle, Liquid Penetrant, Eddy-Current, Ultrasonic, Radiographic, Acoustic Emission), Method, Service, Vertical, and Geography—Global Forecast to 2024*. MarketandmarketsSE 2860. [Online]. Available: https://www.marketsandmarkets.com/Market-Reports/non-destructive-testing-ndt-equipment-services-market-882.html

[2] V. E. Kananen, J. J. Eskelinen, and E. O. Hæggström, "Discriminating pores from inclusions in rolled steel by ultrasonic echo analysis," *Meas. Sci. Technol.*, vol. 22, no. 10, Aug. 2011, Art. no. 105704.
[3] S. Gholizadeh, "A review of non-destructive testing methods of composite materials," *Procedia Struct. Integrity*, vol. 1, pp. 50–57, Feb. 2016.
[4] K. A. Reddy, "Non-destructive testing, evaluation of stainless steel materials," *Mater. Today, Proc.*, vol. 4, no. 8, pp. 7302–7312, 2017.
[5] Y. Zhang, K. Sekine, and S. Watanabe, "Magnetic leakage field due to subsurface defects in ferromagnetic specimens," *NDT E Int.*, vol. 28, no. 2, pp. 67–71, Apr. 1995.
[6] U. Ewert, "Advances in digital industrial radiology—New application areas beyond film radiography," in *Proc. AIP Conf.*, 2013, vol. 1511, no. 1, pp. 18–32.
[7] T. Menaria and M. Kumar, "Review on radiographic imaging modalities for non-destructive testing and evaluation (NDT & E)," in *Proc. Int. Conf. Sustain. Comput. Sci., Technol. Manage. (SUSCOM)*, Jaipur, India, 2019, pp. 1298–1304.
[8] B. L. Luk and A. H. S. Chan, "Human factors and ergonomics in dye penetrant and magnetic particles nondestructive inspection methods," *Eng. Lett.*, vol. 15, no. 1, pp. 163–169, 2007.
[9] J. García-Martín, J. Gómez-Gil, and E. Vázquez-Sánchez, "Non-destructive techniques based on eddy current testing," *Sensors*, vol. 11, no. 3, pp. 2525–2565, Dec. 2011.
[10] R. Guilizzoni, G. Finch, and S. Harmon, "Subsurface corrosion detection in industrial steel structures," *IEEE Magn. Lett.*, vol. 10, 2019, Art. no. 2108005.
[11] D. Chen, H. F. Xiao, M. Li, and J. W. Xu, "A study on the inclusion sizing using immersion ultrasonic C-scan imaging," *J. Phys., Conf. Ser.*, vol. 842, May 2017, Art. no. 012003.
[12] E. D. Mackey and T. F. Seacord, "Guidelines for using stainless steel in the water and desalination industries," *J.-Amer. Water Works Assoc.*, vol. 109, no. 5, pp. E158–E169, May 2017.
[13] P. C. R. Bhagi, "Magnetic flux leakage technique: Basics," *J. Non Destructive Test. Eval.*, vol. 11, pp. 7–17, Dec. 2012.
[14] Y. Li, G. Y. Tian, and S. Ward, "Numerical simulation on magnetic flux leakage evaluation at high speed," *NDT E Int.*, vol. 39, no. 5, pp. 367–373, Jul. 2006.
[15] B. Wolter, G. Dobmann, and I. Fraunhofer, "Micromagnetic testing for rolled steel," in *Proc. 9th Eur. Conf. Non-Destructive Test.*, 2006, pp. 1–11.
[16] W. S. Singh, B. P. C. Rao, S. Thirunavukkarasu, and T. Jayakumar, "Flexible GMR sensor array for magnetic flux leakage testing of steel track ropes," *J. Sensors*, vol. 2012, Mar. 2012, Art. no. 129074.
[17] P. Wang, Y. Gao, G. Tian, and H. Wang, "Velocity effect analysis of dynamic magnetization in high speed magnetic flux leakage inspection," *NDT E Int.*, vol. 64, pp. 7–12, Jun. 2014.
[18] S. Lu, J. Feng, F. Li, and J. Liu, "Precise inversion for the reconstruction of arbitrary defect profiles considering velocity effect in magnetic flux leakage testing," *IEEE Trans. Magn.*, vol. 53, no. 4, pp. 1–12, Apr. 2017.
[19] D. Wu, Z. Liu, X. Wang, and L. Su, "Composite magnetic flux leakage detection method for pipelines using alternating magnetic field excitation," *NDT E Int.*, vol. 91, pp. 148–155, Oct. 2017.
[20] J.-G. Zhu and C. Park, "Magnetic tunnel junctions," *Mater. Today*, vol. 9, no. 11, pp. 36–45, Nov. 2006.
[21] X.-F. Han, "TMR and AI-O based magnetic tunneling junctions," in *Handbook of Spintronics*. Dordrecht, The Netherlands: Springer, 2016, pp. 179–225, doi: 10.1007/978-94-007-6892-5_10.
[22] E. G. Vidal, D. R. Muñoz, S. I. R. Arias, J. S. Moreno, S. Cardoso, R. Ferreira, and P. Freitas, "Electronic energy meter based on a tunnel magnetoresistive effect (TMR) current sensor," *Materials*, vol. 10, no. 10, p. 1134, Sep. 2017.
[23] B. Wu, Y. J. Wang, X. C. Liu, and C. F. He, "A novel TMR-based MFL sensor for steel wire rope inspection using the orthogonal test method," *Smart Mater. Struct.*, vol. 24, no. 7, Jul. 2015, Art. no. 075007.
[24] K. Tsukada, M. Hayashi, Y. Nakamura, K. Sakai, and T. Kiwa, "Small eddy current testing sensor probe using a tunneling magnetoresistance sensor to detect cracks in steel structures," *IEEE Trans. Magn.*, vol. 54, no. 11, pp. 1–5, Nov. 2018.
[25] B. Wang and X. Wang, "A precise magnetic flux leakage method for the defects detection within the steel thin sheet," *IOP Conf. Ser., Mater. Sci. Eng.*, vol. 424, no. 1, Oct. 2018, Art. no. 012010.
[26] J. Zhang, F. Peng, and J. Chen, "Quantitative detection of wire rope based on three-dimensional magnetic flux leakage color imaging technology," *IEEE Access*, vol. 8, pp. 104165–104174, 2020.
[27] G. Balachandran, "Challenges in special steel making," *IOP Conf. Ser., Mater. Sci. Eng.*, vol. 314, no. 1, 2018, Art. no. 012016.
[28] J. Atzlesberger, B. G. Zagar, R. Cihal, M. Brummayer, and P. Reisinger, "Sub-surface defect detection in a steel sheet," *Meas. Sci. Technol.*, vol. 24, no. 8, Jul. 2013, Art. no. 084003.
[29] K. Fujiwara, Y. Okamoto, A. Kameari, and A. Ahagon, "The Newton-Raphson method accelerated by using a line search–comparison between energy functional and residual minimization," *IEEE Trans. Magn.*, vol. 41, no. 5, pp. 1724–1727, May 2005.
[30] P. Bloomfield and W. Steiger, "Least absolute deviations curve-fitting," *SIAM J. Sci. Stat. Comput.*, vol. 1, no. 2, pp. 290–301, Jun. 1980.
[31] A. Kaur, L. Kaur, and S. Gupta, "Image recognition using coefficient of correlation and structural SIMilarity index in uncontrolled environment," *Int. J. Comput. Appl.*, vol. 59, no. 5, pp. 32–39, Dec. 2012.

JOONGHO AHN (Graduate Student Member, IEEE) received the B.S. degree in electronic engineering from Kyungbook National University, South Korea, in 2016. He is currently pursuing the Ph.D. degree in convergence IT engineering with the Pohang University of Science and Technology, South Korea.

His research interests include imaging systems of photoacoustics, ultrasonics, optics, and magnetics, and their combinations for biomedical and industrial applications.

JINHWAN BAIK received the B.S. degree in electronic engineering from Soongsil University, South Korea, in 2017. He is currently pursuing the Ph.D. degree in convergence IT engineering with the Pohang University of Science and Technology, South Korea.

His research interests include system-on-chip for real-time applications and numerical analysis.

CHULHONG KIM (Senior Member, IEEE) received the Ph.D. degree from Washington University in St. Louis, St. Louis, MO, USA.

He is currently the Mueunjae Chair Professor of electrical engineering and convergence IT engineering with the Pohang University of Science and Technology, South Korea.

Prof. Kim was a recipient of the Nightingale Award from the IFMBE in 2016, the IEEE EMBS Early Career Achievement Award in 2017, the Korean Academy of Science and Technology Young Scientist Award in 2017, and the KOSOMBE Young Investigator Award Contributions to Multi-Scale Photoacoustic Imaging from Super-Resolution Atomic Force Photoactivated Microscopy for Research to Systems for Clinical Applications in 2017.

SUNG-MIN PARK (Member, IEEE) received the B.S. and Ph.D. degrees in electrical and computer engineering from Purdue University, West Lafayette, IN, USA, in 2001 and 2006, respectively.

From 2006 to 2014, he was with Medtronic, Minneapolis, MN, USA, as the Research and Development Manager, leading the award-wining effort in developing the world first MRI conditional pacemaker. From 2014 to 2016, he was with Samsung, Suwon, South Korea, as the Director, spearheading healthcare centric mobile device and mobile health service platform development projects. Since 2016, he has been with the Pohang University of Science and Technology (POSTECH), Pohang, South Korea, where he is currently a Professor with the Department of Convergence IT Engineering and Electrical Engineering.